ACCOUNTS of chemical research

Article

pubs.acs.org/accounts

Advanced Electrochemistry of Individual Metal Clusters Electrodeposited Atom by Atom to Nanometer by Nanometer

Published as part of the Accounts of Chemical Research special issue "Nanoelectrochemistry".

Jiyeon Kim,[†] Jeffrey E. Dick,[‡] and Allen J. Bard*[,‡]

[†]Department of Chemistry, The University of Rhode Island, Kingston, Rhode Island 02881, United States

[‡]Center for Electrochemistry, Department of Chemistry, The University of Texas at Austin, Austin, Texas 78712, United States

CONSPECTUS: Metal clusters are very important as building blocks for nanoparticles (NPs) for electrocatalysis and electroanalysis in both fundamental and applied electrochemistry. Attention has been given to understanding of traditional nucleation and growth of metal clusters and to their catalytic activities for various electrochemical applications in energy harvesting as well as analytical sensing. Importantly, understanding the properties of these clusters, primarily the relationship between catalysis and morphology, is required to optimize catalytic function. This has been difficult due to the heterogeneities in the size, shape, and surface properties. Thus, methods that address these issues are necessary to begin understanding the reactivity of individual catalytic centers as opposed to ensemble measurements, where the effect of size and morphology on the catalysis is averaged out in the measurement.

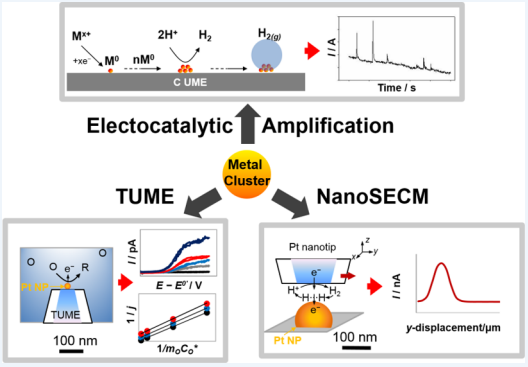

This Account introduces our advanced electrochemical approaches to focus on each isolated metal cluster, where we electrochemically fabricated clusters or NPs atom by atom to nanometer by nanometer and explored their electrochemistry for their kinetic and catalytic behavior. Such approaches expand the dimensions of analysis, to include the electrochemistry of (1) a discrete atomic cluster, (2) solely a single NP, or (3) individual NPs in the ensemble sample. Specifically, we studied the electrocatalysis of atomic metal clusters as a nascent electrocatalyst via direct electrodeposition on carbon ultramicroelectrode (C UME) in a femtomolar metal ion precursor. In addition, we developed tunneling ultramicroelectrodes (TUMEs) to study electron transfer (ET) kinetics of a redox probe at a single metal NP electrodeposited on this TUME. Owing to the small dimension of a NP as an active area of a TUME, extremely high mass transfer conditions yielded a remarkably high standard ET rate constant, k^0, of 36 cm/s for outer-sphere ET reaction. Most recently, we advanced nanoscale scanning electrochemical microscopy (SECM) imaging to resolve the electrocatalytic activity of individual electrodeposited NPs within an ensemble sample yielding consistent high k^0 values of ≥2 cm/s for the hydrogen oxidation reaction (HOR) at different NPs. We envision that our advanced electrochemical approaches will enable us to systematically address structure effects on the catalytic activity, thus providing a quantitative guideline for electrocatalysts in energy-related applications.

1. INTRODUCTION

We are just entering the era of "digital chemistry", where molecules and other entities are fabricated or synthesized one at a time and characterized individually, where characterization includes determination of properties, recognition of the entity, and studies of the chemistry that occurs. While such an approach is not amenable to applications where macroscopic amounts of material are required, it can provide analytical methods with unprecedented sensitivity as well as the possibility of understanding and manipulating structural effects on reactivity.

For example, we consider here metal clusters as building blocks for NPs and their use as electrocatalysts and in analysis. Metal clusters can be categorized into different sizes, shapes, compositions, and factors such as capping agents or cross-linkers. Due to these heterogeneous aspects, understanding the properties of these clusters, mainly their relations to structure and composition, is required for manipulating and optimizing their function. In fact, most ensemble measurements average over a large number of particles, which is completely different from an inherent activity of a single cluster. It however is not trivial to synthesize and characterize metal clusters discretely under a dispersed condition. A big challenge here remains in studying these relations at the individual level especially when we have (1) heterogeneity in the size, shape, composition, and interparticle spacing of metal clusters in an ensemble system and (2) lack of spatial resolution in an analytical approach. At this stage, it becomes obvious that a reliable way of

Received: July 1, 2016
Published: October 27, 2016

DOI: 10.1021/acs.accounts.6b00340
Acc. Chem. Res. 2016, 49, 2587−2595

quantitatively determining the activity and morphology of individual metal clusters is needed.

2. ATOM-BY-ATOM ELECTRODEPOSITION VIA COLLISIONS

Methodology for carrying out an electrodeposition on an atom-by-atom process can provide a new approach to catalyst fabrication. It is also applicable to the analysis of very low concentrations of metal ions and probing the early stages of nucleation and growth of metal deposits. The produced NPs are useful in studying size and structure effects on single particle behavior such as electrocatalytic activity compared to ensemble measurements.

Experiments in Pt atom-by-atom deposition have originated in earlier studies looking at the collision of Pt NPs onto a relatively inert electrode surface, which is termed electrocatalytic amplification (EA).[1] The detectable NP size using this method ranges from 4 to 70 nm in radius. One experiment, shown in Figure 1a, uses a carbon fiber ultramicroelectrode (C

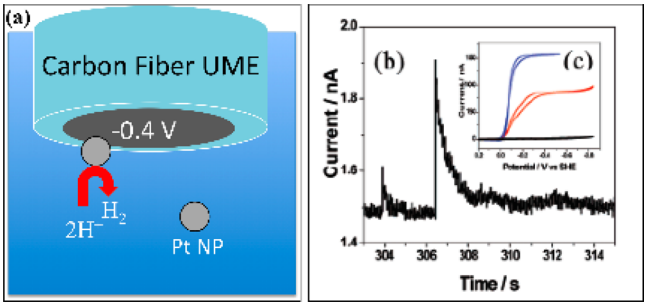

Figure 1. (a) Schematic representation of the collision experiment, (b) current transients at a C UME in 10 mM perchloric acid and 20 mM sodium perchlorate in the presence of Pt citrate NPs, and (c) cyclic voltammograms of C UME (black) and Pt UME in 50 mM sodium dihydrogencitrate (red) and 10 mM perchloric acid and 20 mM sodium perchlorate.[4]

UME), which is inert to a wide range of inner-sphere reactions, placed in a slightly acidic solution. Figure 1b shows the difference in proton reduction between a bare C UME and a C UME decorated with platinum NPs.[1] If the C UME is biased at a potential where proton reduction occurs not on carbon but readily on platinum, a faradaic response can be observed when a platinum NP collides with, and sticks to the C UME.

In collisions, much can be learned from the frequency of collision, the height of the faradaic response, and the shape of the response. Because of the stochastic collision of a NP onto an UME, mass transfer to the electrode is represented by an average collision frequency given by[2]

$$f_{dif} = 4D_{NP}C_{NP}aN_A \quad (1)$$

where f_{dif} is the collision frequency governed by diffusion of the NP to the electrode, D_{NP} is the diffusion coefficient of the NP, C_{NP} is the concentration of NPs, a is the radius of the UME, and N_A is Avogadro's number. From this equation, one can obtain the concentration of NPs or the diffusion coefficient of the NPs. The height of the peak under mass transfer control is given by

$$i_{ss} = 4\pi nFD_H C_H r_{NP} \ln(2) \quad (2)$$

where i_{ss} is the steady-state current for the NP, D_H is the diffusion coefficient of the reactant, for example, proton, n is the stoichiometric number of electrons, F is Faraday's constant, C_H is the proton concentration, and r_{NP} is the NP radius.

Using these collisions, it is possible to get information on the size of the NP with known D and concentration of reactant. This approach, however, has not been applied to determining the kinetics and catalytic properties of single particles for several reasons. First, the synthesis of NPs often leaves a distribution of sizes and shapes. To make a direct electrochemical comparison, relatively monodisperse samples of NPs are necessary. Second, the current response in the amperometric $i-t$ trace often decays over time, implying some type of deactivation process.[3] Third, NPs tend to aggregate in solution with time. Other complex effects on catalysis also exist, such as heterogeneities on electrode surfaces, adsorption of molecular impurities, and the capping agent.

We can apply the same principles of EA with NP collisions to electrodeposited clusters or NPs with developing conditions under which single ion collisions are sensitively monitored.[4] When a single ion is reduced at the electrode surface, the amount of charge passed from a few electrons is too small to be observable in amperometry. However, if the reduction product readily catalyzes a reaction, such as a proton reduction to hydrogen gas, a faradaic response becomes observable. We carry out the reaction in femtomolar $PtCl_6^{2-}$ in 1 M H_2SO_4 on a 10 μm diameter C UME. The potential of the C UME is adjusted sufficiently negative (cathodic) to reduce proton at Pt. Also, at this negative potential, each collision of a $PtCl_6^{2-}$ onto C UME will result in electrodeposition of platinum atom by atom. At femtomolar concentrations, the diffusion rate of ions to the electrode is on the order of one ion per 5−10 s. The time for proton reduction to occur is a measure of the number of Pt atoms deposited. If this follows a nucleation and growth mechanism, a small cluster of Pt atoms could form.

Figure 2a shows representative data. Each proton reduction event is marked by a sharp increase in current and a fast decay. White and co-workers have reported nanobubble formation on the surface of nanometer platinum electrodes in high concentrations of acid.[5] In their experiment, a bubble nucleates, grows, and stays stable as long as the potential is held sufficiently negative to reduce protons. They speculate that a small ring around the electrode continues to reduce protons to hydrogen at a rate equal to the rate of hydrogen dissolving at the edge of the bubble. This ring was estimated to be ca. 10 pm. Based on their studies, we propose that a bubble forms on the catalytic center and effectively isolates the cluster and shuts the catalysis off. Figure 2b shows the average experimental frequency as a function of concentration of $PtCl_6^{2-}$ (solid line). The dashed line represents the frequency of collision of $PtCl_6^{2-}$ anions calculated using eq 1. From the plots, the difference in slope is a factor of 5, implying that on the average, 5 ± 1 ions of $PtCl_6^{2-}$ have interacted with the C UME surface when an event is observed. We assume that the electrodeposition of atoms follows the classical nucleation and growth model, where one can nucleate and grow single catalytic centers on UMEs shown by Fleischmann[6] and Kucernak.[7] This ratio may suggest that the electrocatalyst cluster contains five Pt atoms. One other novel way of controlling the flux of molecule to the electrode surface is by trapping the molecules in a droplet in an emulsion setup.

The ability to calculate the catalyst size in this manner depends on a number of assumptions and requires several caveats. The nucleation and growth model in this case requires that (1) the platinum atoms remain on the C surface, (2) the

DOI: 10.1021/acs.accounts.6b00340
Acc. Chem. Res. 2016, 49, 2587−2595

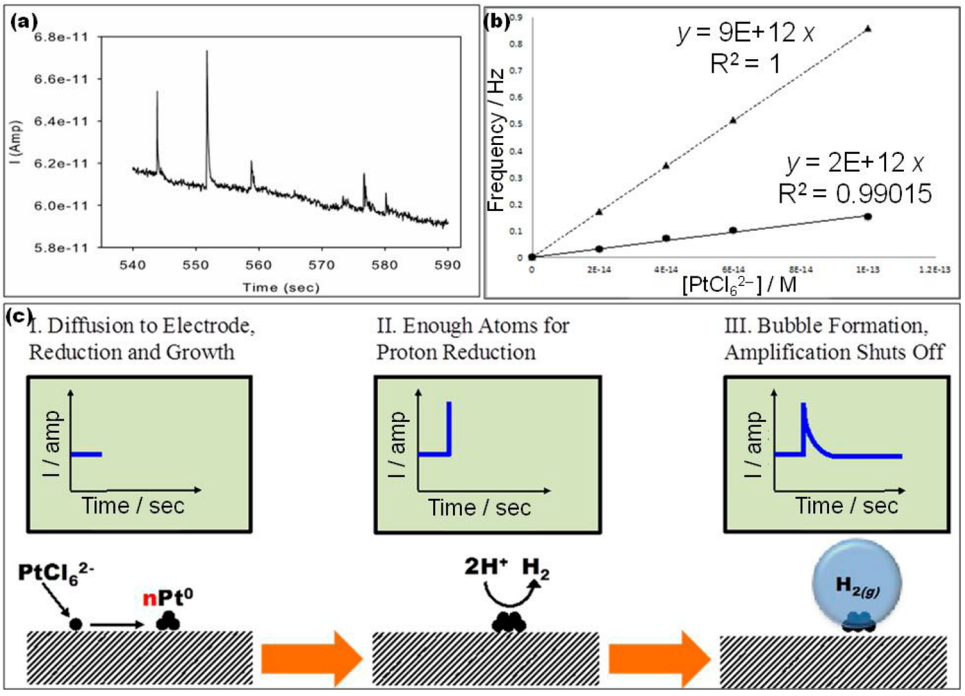

Figure 2. (a) Proton reduction peaks resulting from electrodeposition of platinum from femtomolar concentrations in H_2SO_4. (b) Average experimental frequency as a function of concentration of hexachloroplatinic acid (solid line) plotted with the calculated frequency from eq 1 per hexachloroplatinate anion. (c) Proposed model.

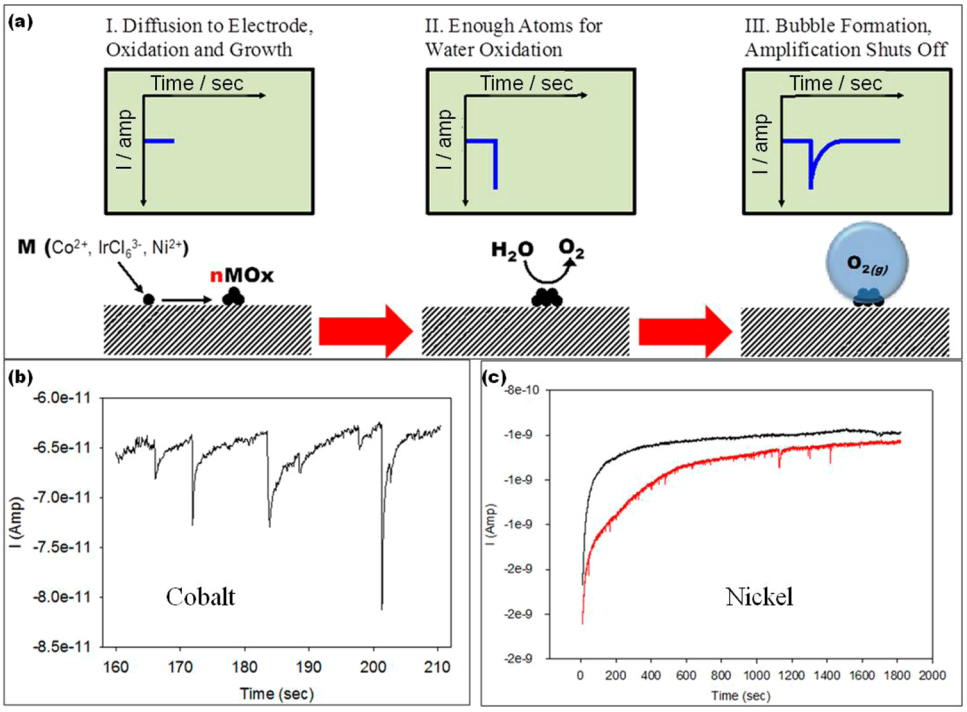

Figure 3. (a) Schematic representation of the oxidation experiments. (b,c) Representative current−time traces for 62 fM cobalt ion and 100 fM nickel ion on a C UME, respectively.

size of the electrode is small enough to have only a single nucleation site on the surface, and (3) the atoms move rapidly on the surface until they find the nucleation site. Also, the nature of the surface (material and structure) can affect the size and the number of atoms. Capping agents and adsorbed impurities will affect catalytic properties and the size. We recognize that the redox potential of a single platinum atom is different from bulk material,[8] and we assume the potential at hydrogen evolution (~1000 mV more negative than potential of reduction of hexachloroplatinate to bulk platinum) is sufficient to drive the electrodeposition reaction under mass transfer control. For reliable analysis, the electrode is often calibrated by taking a cyclic voltammogram of an inner-sphere (such as hydrazine oxidation) and outer-sphere (such as

DOI: 10.1021/acs.accounts.6b00340
Acc. Chem. Res. 2016, 49, 2587−2595

ferrocene methanol oxidation) reaction to ensure a consistent electrode size. Inherently, complications arise due to two different nucleation and growth events in our current model: a single catalytic center and a hydrogen bubble.

3. COLLISIONS OF OER CATALYSTS

We explored the possibility to nucleate catalysts capable of water oxidation, such as cobalt oxide, iridium oxide, and nickel oxide doped with iron.[9] Figure 3 shows the experimental scheme as well as representative data. The anodic oxidation in a solution of the metal ion (i.e., Co^{2+}, Ni^{2+}) is known to form an oxide that is catalytic for oxygen evolution reaction (OER) by water oxidation. These ions at femtomolar level can be electrodeposited as an oxide under sufficiently positive potential and cause oxygen evolution. Each water oxidation event is marked by a sharp increase in current, and then followed by decay due to the formation of an oxygen bubble on the catalyst. Through a similar frequency versus concentration analysis, the number of metal ions necessary to catalyze water oxidation was estimated as 10 ions of cobalt and 11 ions of nickel. In bulk catalytic studies, it is well-known that the oxidation of water by nickel is enhanced by the addition of iron.[10] When femtomolar solutions of nickel and iron are mixed together, the observed current peak height reaches a maximum under the ratio of nickel to iron 5:1. This result is interesting considering that the stochastic technique gives similar information to bulk catalytic measurements.[10]

4. TUNNELING ULTRAMICROELECTRODE: AS USED TO STUDY THE ET KINETICS AT A SINGLE NP

In this section, we expand our scope to a nanometer-sized metal cluster and hence demonstrate tunneling ultramicroelectrodes (TUMEs) as a versatile platform to study the electrochemistry of a single NP. A TUME involves a thin film of a dielectric on a conducting surface as an electrode.[11] For example, a TiO_2 film is electrodeposited on the conducting Pt surface of a UME to block a direct ET to solution species. The film is thin enough, ca. 1 nm, to allow tunneling to a Pt NP. Thus, the subsequent contact of metal NP to the TiO_2 film restores the direct ET to solution species solely on the NP via facile electron tunneling. Consequently, the composite of UME/TiO_2 film/NP offers a nanometer scale active area. By applying a high enough potential on the TUME, we can also drive the ET reaction across the TiO_2 layer and thus directly electrodeposit a metal NP on the TUME resulting in a new nanometer-sized electrode as shown in Figure 4. This approach allowed for fabrication of electrodes with radii of a few to tens of nanometers.

A single Pt NP was visually confirmed by scanning electron microscopy (SEM) and a focused ion beam (FIB). In Figure 5, ca. 13 nm and 28.5 nm radius single Pt NPs on each TUME were seen with nearly spherical geometry, consistent with the estimated radii from the integrated charges during current–time transient.

Owing to the pinhole free TiO_2 layer, a Pt NP on the TUME (Pt NP/TUME) could be electrochemically characterized by steady state voltammetry in 5 mM $Ru(NH_3)_6^{3+}$, where the Pt NP is solely responsible for the current response. Thereby, the radius of the Pt NP on the TUME was estimated from a limiting current in obtained voltammograms assuming a single Pt NP with a spherical geometry on a planar surface,[11]

$$i_{lim} = 4\pi(\ln 2)nFDC^*r \quad (3)$$

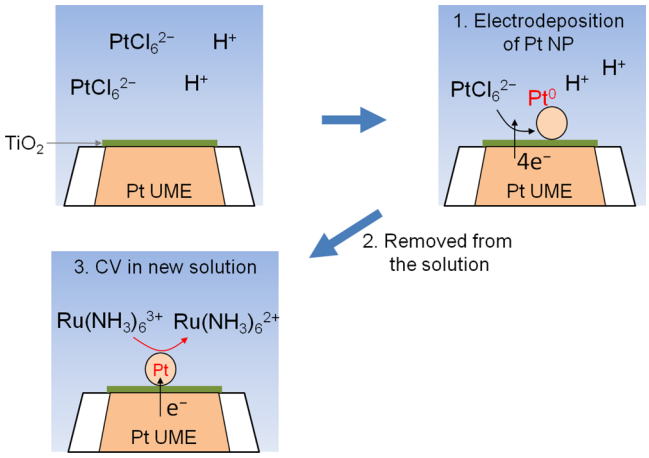

Figure 4. Schematics of the fabrication and the characterization of Pt NP/TUME by electrodepositing a single Pt NP on TUME, removal of Pt NP/TUME from the solution, and running cyclic voltammetry (CV) in new solution of $Ru(NH_3)_6^{3+}$.

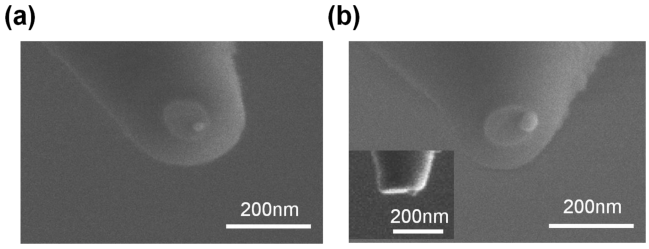

Figure 5. SEM images of (a) ca. 13 nm and (b) 28.5 nm radius Pt NPs on TUMEs. In inset of FIB image, the side view of Pt NP on TUME is shown.

where i_{lim} is a limiting current, F is the Faraday constant (96485 C/mol), D is a diffusion coefficient of $Ru(NH_3)_6^{3+}$ (7.4×10^{-6} cm^2/s), C^* is a bulk concentration (5 mM) with the transferred electron number, $n = 1$, and r is a radius of a single Pt NP. The resulting radii of Pt NPs range from 0.7 to 41.6 nm for the given voltammograms in Figure 6 (the rationalization of the single NP presence on TUME can be found in ref 12).

Varying the size of the Pt NP, that is, the electrode size in this work, is equivalent to altering the mass transfer rate, m. Hence, we employ an UME treatment equivalent to the Kotecký–Levich (K-L) RDE method but demonstrated for general UMEs,[12] where a series of steady state voltammograms from different sizes of Pt NP/TUMEs are used to construct a plot of 1/current density (j) vs $1/m$ at different potentials to extract the kinetic information. We applied a Pt NP/TUME to a kinetic study of heterogeneous ET reaction of $Ru(NH_3)_6^{3+}$ as a model redox mediator using steady state voltammetry.

Because of the efficient electron tunneling across a ca. 1 nm thick TiO_2 layer, the overall current density, j, at a Pt NP in the K-L treatment can be expressed as

$$\frac{1}{j} = \frac{1}{j_{et}} + \frac{1}{j_{mt}} \quad (4)$$

for a quasi-reversible one-step one electron reduction reaction,

$$O + e^- \underset{k_b}{\overset{k_f}{\rightleftarrows}} R \quad (5)$$

The overall current density can be written as equation[12]

DOI: 10.1021/acs.accounts.6b00340
Acc. Chem. Res. 2016, 49, 2587–2595

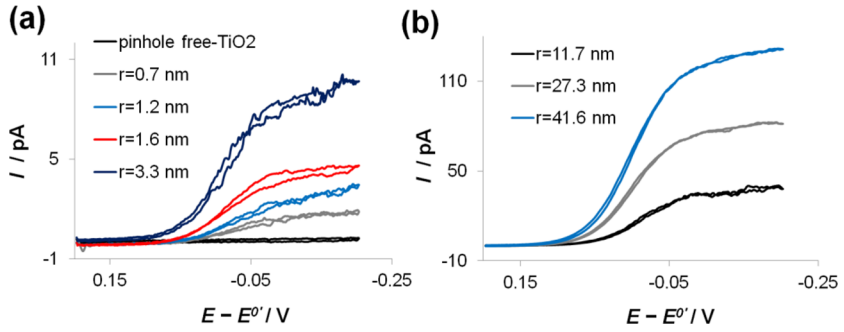

Figure 6. Cyclic voltammograms of (a) bare TUME with a pinhole free TiO_2 layer and radii of 0.7 to 3.3 nm Pt NP/TUME and (b) radii of 11.7 to 41.6 nm Pt NP/TUME in 5 mM $Ru(NH_3)_6^{3+}$, 0.1 M KNO_3.

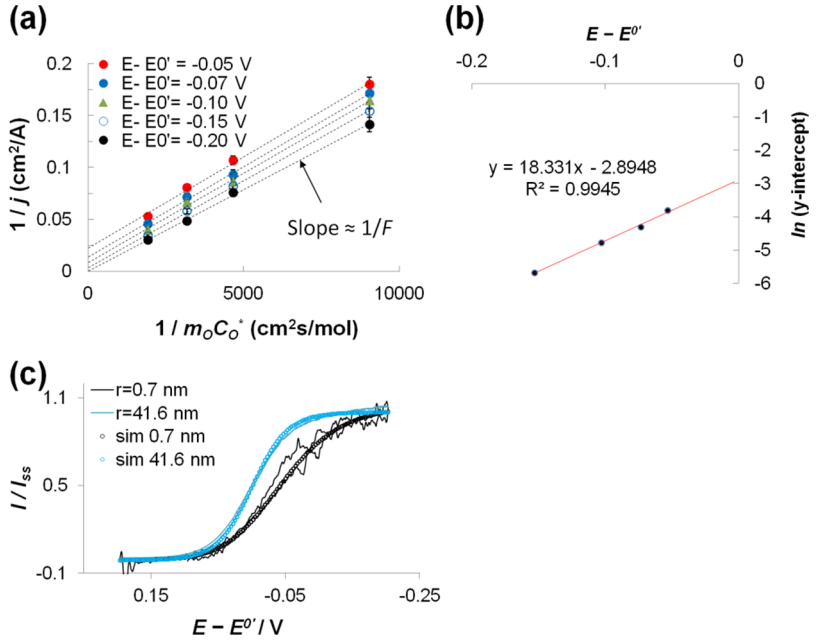

Figure 7. (a) K–L plots generated from CVs in Figure 6a, (b) linear plot of ln(y-intercept) vs (E–$E^{0\prime}$) obtained from K–L analysis. Both α and k^0 could be independently determined from the obtained slope and new y-intercept, respectively. (c) Theoretically simulated voltammograms (open circles) for k^0 = 36 cm/s, α = 0.5 fitted with experimental curves (solid lines) from radii of 0.7 and 41.6 nm Pt NP/TUMEs. Each voltammogram was normalized with respect to its limiting current.

$$\frac{1}{j} = \frac{1}{Fk^0C^*}\frac{(b)^\alpha}{(1-pb)} + \frac{1}{FmC^*}\left(\frac{1+qb}{1-pb}\right) \quad (6)$$

where

$$b = e^{F/RT(E-E^{0'})}, \quad C^* = C_O^*, \quad C_R^* = pC_O^*, \quad m = m_O,$$

and $\quad m_O/m_R = q$

Notably, eq 6 is analogous to eq 4 of K-L treatment; thereby we can construct a plot of $1/j$ vs $1/(mC^*)$ at given different potentials similar to conventional K-L plot. A set of linear K-L plots are obtained with a constant slope of $\sim 1/F$ and different y-intercepts as presented in Figure 7a, where potential ranges of $E - E^{0\prime} \leq -0.05$ V are used in CVs from 0.7 to 3.3 nm radius Pt NP/TUMEs. In this potential range, b becomes close to 0; thus a resulting slope of all K-L plots should be $1/F$. At large potential such as −0.2 V, mass transfer dominates, so that a linear K-L plot intersects the origin. As the potential becomes smaller, the y-intercept, $\frac{1}{Fk^0C^*}\frac{(b)^\alpha}{(1-pb)}$, deviates more from the origin due to a greater contribution of kinetic control. From a set of y-intercepts in the potential range from −0.15 to −0.05 V, we could estimate k^0 remarkably high as 36 ± 4 cm/s with α = 0.47, where p = 0.01 to 0.001 based on a nearly zero initial current in CVs and q = 1 are assumed. Herein, α was numerically determined from the potential dependence of the y-intercepts but independent of the k^0 value. Because the y-intercept = $\frac{1}{Fk^0C^*}\frac{(b)^\alpha}{(1-pb)}$ and $pb \ll 1$, we can derive the equation as,

$$\ln(y\text{-intercept}) = \ln\left(\frac{1}{Fk^0C^*}\right) + \frac{\alpha F}{RT}(E - E^{0\prime}) \quad (7)$$

By plotting ln(y-intercept) vs ($E - E^{0\prime}$), both α and k^0 could be independently determined from the corresponding slope and new y-intercept, respectively (Figure 7b).

The measured kinetic parameters were further confirmed with finite element analysis using COMSOL MULTIPHYSICS (v. 4.2a). As presented in Figure 7c, the simulated voltammograms for k^0 = 36 cm/s, α = 0.5, fit well with experimental curves from the smallest, 0.7 nm, to the largest radius, 41.6 nm, of Pt NP/TUME, which shows a clear transition from kinetic

DOI: 10.1021/acs.accounts.6b00340
Acc. Chem. Res. 2016, 49, 2587−2595

control to almost Nernstian behavior. These result are consistent with the exceptionally high k^0 determined here for $Ru(NH_3)_6^{3+}$.

Particle size effects on the relative rate constants are also of interest. The present approach will be particularly useful in that direction, because the constraint of the slope, $1/F$ in K-L plot can be used to evaluate whether the present ET system deviates from linearity, that is, size effects exist especially as the NP or nanoelectrode becomes smaller. Note that within the particle range given in Figure 7a, we found no dependence of k^0 on particle radius. Importantly, this is the first experimental approach to reliably evaluate the size effect on simple outer-sphere ET kinetics, where the protruded geometry of NP on TUME and an extremely high purity solution avoid the over- or underestimation, whereas a recession of planar electrode or impurities in the solution can lead to such over- or underestimation[13,19] thus causing an apparent size effect.

5. NANOSCALE SECM: A VERSATILE NANOSCALE METHOD FOR THE STUDY OF ELECTROCATALYSIS AT INDIVIDUAL NANOPARTICLES WITHIN AN ENSEMBLE SAMPLE

Generally NPs exist as arrays in ensembles on the support substrate with heterogeneities in their size, shape, spatial orientation, and catalytic activity. In this section, we introduce advanced nanoscale SECM imaging to resolve the geometric property and catalytic activity of individual NPs even within an ensemble sample. SECM is an imaging technique providing chemical and topographic information, especially about surfaces immersed in a solution by moving a small (micrometer to nanometer sized) tip electrode very close to a substrate surface.

Herein, Pt NPs with a few tens to 100 nm radius were directly electrodeposited on highly oriented pyrolytic graphite (HOPG) via nucleation and growth electrodeposition without the necessity for capping agents or anchoring molecules. Well-defined hemisphere to sphere shaped Pt NPs with 90 ± 30 nm radii were observed by field emission-SEM (FE-SEM) in Figure 8a. A uniform height of ca. 120 nm was seen while various aspect ratios were measured, indicating that Pt NPs are spread out once they reach a steady state height during nucleation and growth (Figure 8a, bottom). Additionally, highly preferential deposition of the NPs along the edge plane of HOPG was observed as reported by Penner and co-workers.[14] The NPs were well resolved without aggregation as required for SECM measurements at an individual NP level.

We employed nanoscale SECM with an inlaid disk Pt nanotip to map electrochemical activity at individual NPs. To resolve the topographic information and electrochemical activity of Pt NPs, we performed two consecutive SECM experiments using two different redox mediators, (1) $FcTMA^+$ undergoing outer-sphere ET reaction under mass transfer limiting conditions and (2) H^+ undergoing inner-sphere ET reaction. As schematically shown in Figure 8c, each different ET reaction is studied at the same Pt NPs using a Pt nanotip comparable to the radius of Pt NPs. First, SECM measurements using $FcTMA^+$ are carried out at a distance between the Pt nanotip and substrate surface comparable to the radius of Pt nanotip, where the $FcTMA^{2+}$ generated at the Pt nanotip can be reduced back to $FcTMA^+$ at both HOPG and Pt NPs at a rate governed by diffusion. The heterogeneous ET reaction of this mediator is not sensitive to the catalytic activity of the different surfaces. Thus, the distance between the tip and the target, and hence the topographic factor, only determines the tip current during the SECM imaging at a constant height. The subsequent SECM measurement is carried out using HOR, an inner-sphere ET reaction sensitive to the surface catalytic property.[15] In this case, H_2 molecules generated at the Pt nanotip cannot be oxidized back to H^+ at HOPG but are selectively oxidized at the Pt NP. Accordingly, the tip current over Pt NPs during SECM imaging contains information on the catalytic activity of HOR, as well as topography; thereby a catalytic activity of Pt NP can be solely extracted after resolving the topographic information determined from the study with $FcTMA^+$.

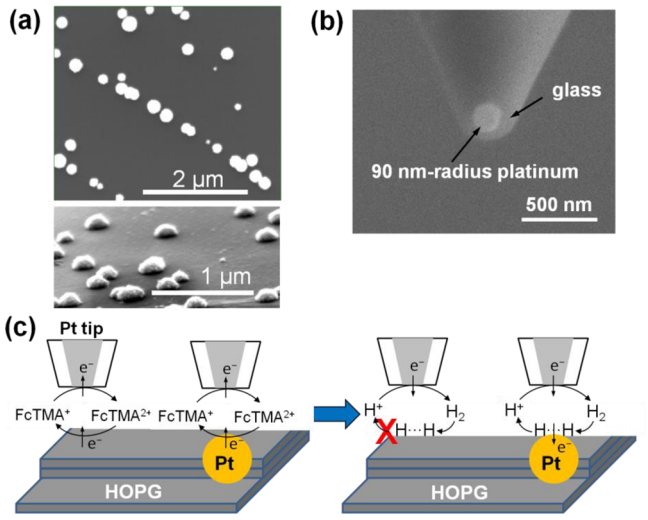

Figure 8. (a) FE-SEM images of electrodeposited Pt NPs on HOPG from top and side view. Pt NPs are preferentially deposited along the edge of HOPG. (b) SEM image of FIB milled Pt nanotip. (c) Schemes illustrating ET reactions occurring at Pt NP and HOPG in the presence of $FcTMA^+$ (left) or H^+ (right). Adapted with permission from ref 16. Copyright 2016 American Chemical Society.

Based on this strategy, the SECM image with $FcTMA^+$ was obtained at a constant height 90 nm above the apex of NPs. Because of a 120 nm uniform height of the electrodeposited NPs confirmed by SEM, the radius of NPs is the only determining factor for the tip current over the Pt NP. Hence, we theoretically predict the tip current−distance curves over the Pt NPs by varying the radii of Pt NPs at the diffusion-controlled condition as shown in Figure 9. By comparing the currents measured in the SECM image at a 90 nm gap, we could determine the radius of the five Pt NPs to be 63, 63, 108, 76, and 117 nm, in order from first to fifth as noted in Figure 10a.

Using the determined NP dimensions, we performed numerical simulations in 3D space to define the spatial orientation of NPs with respect to each other and predict the current vs lateral distance profiles over the NPs. The theoretical currents along the x axis at three different locations (i.e., at a, b, and c in Figure 10a) were simulated and compared with the experimental current profile cross-sectioning the SECM image presented in Figure 10b. Theory and experimental values agree well, validating the determined NP sizes and spatial orientation of NP arrays.

A complementary SECM image with H^+/H_2 was continuously measured at the same location and a constant height 14 nm above the apex of each Pt NP in HOR in Figure 11a. At this 14 nm gap, a theoretical tip current over the Pt NP along the y-

DOI: 10.1021/acs.accounts.6b00340
Acc. Chem. Res. 2016, 49, 2587−2595

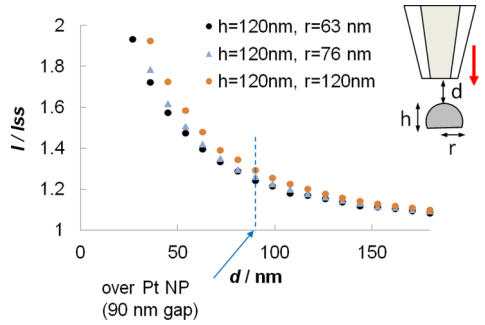

Figure 9. Theoretical current−distance curves for an inlaid-disk tip with RG 2.5 approaching a reactive hemispherical to spherical NP with dimensions, *h* (height) and *r* (radius), on the inert HOPG substrate. *d* represents the gap between the tip and apex of spherical NP. The resulting tip current over the NP is diffusion controlled in this analysis. Reproduced with permission from ref 16. Copyright 2016 American Chemical Society.

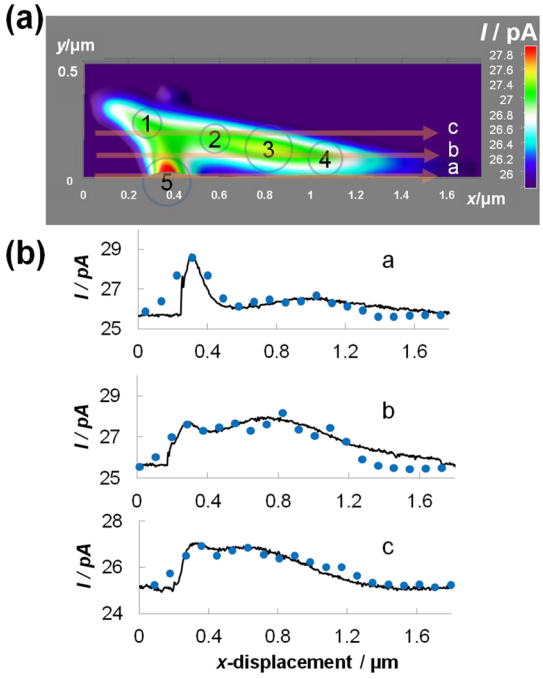

Figure 10. (a) SECM image for $FcTMA^{2+}/FcTMA^{+}$ couple and denoted three different lateral location of a, b, and c for cross-sectioning. (b) Cross-sectional current responses at each different location from SECM image in panel a. The experimental curves (solid lines) show a good fit with theoretical simulation (closed circles), where the ET reaction at Pt NPs is governed by diffusion control in this analysis. Reproduced with permission from ref 16. Copyright 2016 American Chemical Society.

axis was predicted with determined NP dimensions and was compared with the experimental current profiles. In Figure 11b, good agreement in current magnitude over three different Pt NPs is obtained especially under diffusion controlled conditions, implying that H_2 generated at the Pt nanotip is rapidly oxidized at the Pt NPs as soon as it diffuses to the surface (an explicit discussion about the ellipsoidal shaped NPs in SECM image or a discrepancy in current peak width shown in Figure 11 can be found in the ref 16, not discussed here).

Generally, a diffusion-controlled condition is obtained when the corresponding heterogeneous ET rate is at least an order of magnitude larger than the mass transfer rate.[17] Particularly, at

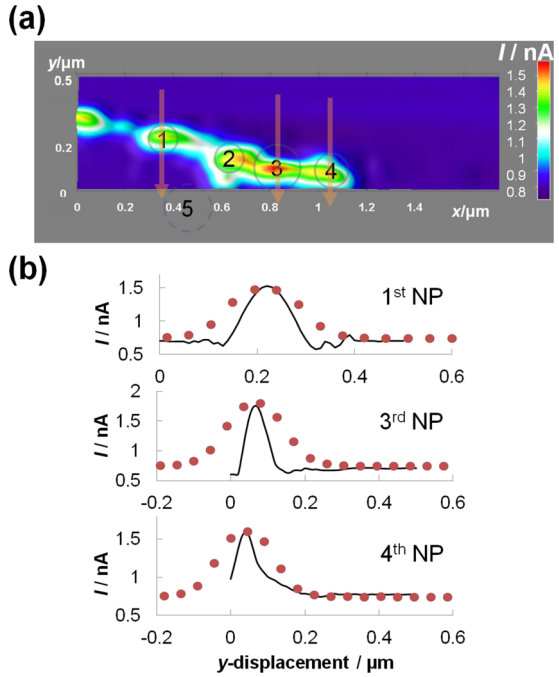

Figure 11. (a) SECM image for H^{+}/H_2 couple and denoted three different locations such as 1st, 3rd, and 4th Pt NPs for cross sectioning in the *y*-axis. (b) Current−distance profiles over each different NP from SECM image in panel a. The experimental curves (solid lines) fit well with theoretical simulation (circular points) in terms of current magnitudes, where the ET reaction at Pt NPs is governed by diffusion control in this analysis. Reproduced with permission from ref 16. Copyright 2016 American Chemical Society.

14 nm gap between tip and the apex of Pt NPs during SECM imaging, the resulting mass transfer rate increases to 26 cm/s ($=D_{H_2}/d$, D_{H_2} = 3.7 × 10^{-5} cm^2/s, d = 14 nm). Using the Butler−Volmer relationship, we could extract a lower limit of the heterogeneous effective rate constant for HOR, $k^0_{eff} \geq 2$ cm/s with $\alpha = 0.5$ and potential difference $(E - E^{0\prime})$ = ca. 250 mV. So far, k^0_{eff} of ≥0.9 cm/s has been reported by Kucernak and co-workers using a floating electrode with Pt NP ensembles under highly enhanced mass transfer conditions.[18] Notably, the large k^0_{eff} in our work was attained at each individual Pt NP not an ensemble. Furthermore, no discernible variation in the reactivity was observed among different sizes of Pt NPs from 63 to 120 nm radii especially under the high purity experimental conditions, whereas significant variation in oxygen reduction activity has been reported depending on the size among electrodeposited Pt NPs studied by scanning electrochemical cell microscopy (SECCM).[19] We speculate that such a variation might come from airborne contaminants on the surface of Pt NPs in SECCM setup originating from the exposure to air. Our experimental conditions include ultrapure water with TOC level <3 ppb, minimum exposure of NP surface to the air, storing the sample in ultrapure water, and an electrochemical cleaning process for the tip and NP surface. Such steps were crucial to the reproducible measurement of the electrocatalytic HOR activity of Pt NPs. Although this study does not show size dependence, a size effect may be found with a larger size variation.[20] Thus, nanoSECM can provide a versatile approach by varying the dimension of NPs, nanotip, and nanogap flexibly up to the tens of nanometer regime.

DOI: 10.1021/acs.accounts.6b00340
Acc. Chem. Res. 2016, 49, 2587−2595

6. CONCLUSIONS AND PERSPECTIVES

In this work, we have suggested three powerful analytical approaches to quantitatively determine the activity and morphology of individual metal clusters at atomic to nanometer resolution. The atom by atom approach using EA has shown high selectivity as well as sensitivity to monitor the atomic sized metal clusters and thus further promises a possibility of detecting significantly low concentrations of metal ions, for example, Pb^{2+}. Moreover, TUME expanded our scope to investigate a nanometer-sized single metal cluster, that is, a NP solely electrodeposited on TUME, and showed successful application along with K-L analysis of an extremely fast ET kinetic study providing a measure of size effect. The extension of this approach to an inner-sphere ET reaction undergoing surface-sensitive electrocatalytic reactions is more complicated but may be able to reveal the heterogeneous and dynamic behavior of metal clusters as catalysts.[21] Flexibility can be gained through electrodepositing various metal NPs[22,23]on TUMEs; thereby this approach should be broadly useful in studying particle composition, size, and structure effects on the catalytic activity of given nanocatalysts.[24,25] Owing to a high spatial resolution of nanoscale SECM, isolated NPs within an ensemble sample could be quantitatively studied for their size, shape, spatial orientation, and catalytic activity at an individual level along with theoretical modeling. Effectively, nanoSECM also can address the surface property effects on the NP's catalytic reactivity, such as capping agent effects for optimum catalytic properties. Overall, we envision that newly developed electrochemical approaches described here will serve as powerful tools to systematically address structure effects on the catalytic activity, thereby providing quantitative guidelines for electrocatalysts in energy-related applications.

■ AUTHOR INFORMATION

Corresponding Author

*E-mail: ajbard@mail.utexas.edu.

Notes

The authors declare no competing financial interest.

Biographies

Jiyeon Kim received B.S. and M.S. degrees from the Ewha Woman's University and Ph.D. at the University of Pittsburgh in 2012. After a postdoctoral position at the University of Texas at Austin, she joined the faculty at the University of Rhode Island in 2016.

Jeffrey E. Dick earned a B.S. in Chemistry from Ball State University in Muncie, Indiana, in 2013. He is currently a National Science Foundation Graduate Research Fellow in the laboratory of Dr. Allen J. Bard at the University of Texas at Austin. His research interests include nanoelectrochemistry, single molecule and NP chemistry, bioelectrochemistry, and the applications of electrochemistry to other areas of academic focus.

Allen J. Bard received a B.S. in Chemistry in 1955 from The City College of New York and received a Ph.D. under the mentorship of J. J. Lingane at Harvard University in 1958. Dr. Bard moved to the University of Texas at Austin in 1958, and he has spent his entire career there.

■ REFERENCES

(1) Xiao, X. Y.; Bard, A. J. Observing Single Nanoparticle Collisions at an Ultramicroelectrode by Electrocatalytic Amplification. *J. Am. Chem. Soc.* **2007**, *129*, 9610−9612.

(2) Kwon, S. J.; Zhou, H.; Fan, F. − R. F.; Vorobyev, V.; Zhang, B.; Bard, A. Stochastic electrochemistry with electrocatalytic nanoparticles at inert ultramicroelectrodes—theory and experiments. *Phys. Chem. Chem. Phys.* **2011**, *13*, 5394−5402.

(3) Bard, A. J.; Zhou, H.; Kwon, S. J. Electrochemistry of Single Nanoparticles via Electrocatalytic Amplification. *Isr. J. Chem.* **2010**, *50*, 267−276.

(4) Dick, J. E.; Bard, A. J. Observation of Single-Protein and DNA Macromolecule Collisions on Ultramicroelectrodes. *J. Am. Chem. Soc.* **2015**, *137*, 13752−13755.

(5) Luo, L.; White, H. S. Electrogeneration of Single Nanobubbles at Sub-50-nm-Radius Platinum Nanodisk Electrodes. *Langmuir* **2013**, *29*, 11169−11175.

(6) (a) Sousa, J. P.; Pons, S.; Fleischmann, M. Studies of silver electronucleation onto carbon microelectrodes. *J. Chem. Soc., Faraday Trans.* **1994**, *90*, 1923−1929. (b) Abyaneh, M. Y.; Fleischmann, M.; Del Giudice, E.; Vitiello, G. The investigation of nucleation using microelectrodes: I. The ensemble averages of the times of birth of the first nucleus. *Electrochim. Acta* **2009**, *54*, 879−887.

(7) Chen, S.; Kucernak, A. Electrodeposition of Platinum on Nanometer-Sized Carbon Electrodes. *J. Phys. Chem. B* **2003**, *107*, 8392−8402.

(8) Henglein, A., Mechanism of Reactions on Colloidal Microelectrodes and Size Quantization Effects. In *Electrochemistry, II*; Steckhan, E., Calabrese, G. S., Eds.; Topics in Current Chemistry, Vol. *143*, Springer-Verlag: Berlin Heidelberg, 1988; Chapter 8, pp 115−175.

(9) Dick, J. E.; Bard, A. J. Unpublished results.

(10) (a) Smith, R. D. L.; Prevot, M. S.; Fagan, R. D.; Trudel, S.; Berlinguette, C. P. Water Oxidation Catalysis: Electrocatalytic Response to Metal Stoichiometry in Amorphous Metal Oxide Films Containing Iron, Cobalt, and Nickel. *J. Am. Chem. Soc.* **2013**, *135*, 11580. (b) Trotochaud, L.; Ranney, J. K.; Williams, K. N.; Boettcher, S. W. Solution-Cast Metal Oxide Thin Film Electrocatalysts for Oxygen Evolution. *J. Am. Chem. Soc.* **2012**, *134*, 17253.

(11) Kim, J.; Kim, B.-K.; Cho, S.-K.; Bard, A. J. Tunneling Ultramicroelectrode: Nanoelectrodes and Nanoparticle Collisions. *J. Am. Chem. Soc.* **2014**, *136*, 8173−8176.

(12) Kim, J.; Bard, A. J. Application of the Koutecký-Levich Method to the Analysis of Steady State Voltammograms with Ultramicroelectrodes. *Anal. Chem.* **2016**, *88*, 1742−1747.

(13) Penner, R. M.; Heben, M. J.; Longin, T. L.; Lewis, N. S. Fabrication and use of nanometer-sized electrodes in electrochemistry. *Science* **1990**, *250*, 1118.

(14) Zoval, J. V.; Lee, J.; Gorer, S.; Penner, R. M. Electrochemical Preparation of Platinum Nanocrystallites with Size Selectivity on Basal Plane Oriented Graphite Surfaces. *J. Phys. Chem. B* **1998**, *102*, 1166−1175.

(15) Zhou, J.; Zu, Y.; Bard, A. J. Scanning electrochemical microscopy: Part 39. The proton/hydrogen mediator system and its application to the study of the electrocatalysis of hydrogen oxidation. *J. Electroanal. Chem.* **2000**, *491*, 22−29.

(16) Kim, J.; Renault, C.; Arroyo-Currás, N.; Nioradze, N.; Leonard, K. C.; Bard, A. J. Electrocatalytic Activity of Individual Pt Nanoparticles Studied by Nanoscale Scanning Electrochemical Microscopy. *J. Am. Chem. Soc.* **2016**, *138*, 8560−8568.

(17) Bard, A. J.; Faulkner, L. R. *Electrochemical Methods: Fundamentals and Applications*, 2nd ed.; John Wiley & Sons: New York, 2001.

(18) Zalitis, C. M.; Sharman, J.; Wright, E.; Kucernak, A. R. Properties of the hydrogen oxidation reaction on Pt/C catalysts at optimized high mass transport conditions and its relevance to the anode reaction in PEFCs and cathode reactions in electrolysers. *Electrochim. Acta* **2015**, *176*, 763−776.

(19) Lai, S. C. S.; Dudin, P. V.; Macpherson, J. V.; Unwin, P. R. Visualizing Zeptomole (Electro)Catalysis at Single Nanoparticles within an Ensemble. *J. Am. Chem. Soc.* **2011**, *133*, 10744−10747.

(20) Auffan, M.; Rose, J.; Bottero, J.-Y.; Lowry, G. V.; Jolivet, J.-P.; Wiesner, M. R. Towards a definition of inorganic nanoparticles from

DOI: 10.1021/acs.accounts.6b00340
Acc. Chem. Res. 2016, 49, 2587−2595

an environmental, health and safety perspective. *Nat. Nanotechnol.* **2009**, *4*, 634−641.
(21) Bard, A. J. Inner-Sphere Heterogeneous Electrode Reactions. Electrocatalysis and Photocatalysis: The Challenge. *J. Am. Chem. Soc.* **2010**, *132*, 7559−7567.
(22) Walter, E. C.; Murray, B. J.; Favier, F.; Kaltenpoth, G.; Grunze, M.; Penner, R. M. Noble and Coinage Metal Nanowires by Electrochemical Step Edge Decoration. *J. Phys. Chem. B* **2002**, *106*, 11407−11411.
(23) Galhenage, R. P.; Yan, H.; Tenney, S. A.; Park, N.; Henkelman, G.; Albrecht, P.; Mullins, D. R.; Chen, D. A. Understanding the Nucleation and Growth of Metals on TiO_2: Co Compared to Au, Ni, and Pt. *J. Phys. Chem. C* **2013**, *117*, 7191−7201.
(24) Zhou, X.; Xu, W.; Liu, G.; Panda, D.; Chen, P. Size-Dependent Catalytic Activity and Dynamics of Gold Nanoparticles at the Single-Molecule Level. *J. Am. Chem. Soc.* **2010**, *132*, 138−146.
(25) Isaifan, R. J.; Ntais, S.; Baranova, E. A. Particle size effect on catalytic activity of carbon-supported Pt nanoparticles for complete ethylene oxidation. *Appl. Catal., A* **2013**, *464*−*465*, 87−94.

DOI: 10.1021/acs.accounts.6b00340
Acc. Chem. Res. 2016, 49, 2587−2595